Anisotropic ferromagnetism in carbon-doped zinc oxide from first-principles studies

Sanjeev K. Nayak,[1,*] Markus E. Gruner,[1] Sung Sakong,[1] Shreekantha Sil,[2] Peter Kratzer,[1] Surjyo N. Behera,[3,†] and Peter Entel[1]

[1]*Faculty of Physics and Center for Nanointegration (CENIDE), University of Duisburg-Essen, 47048 Duisburg, Germany*

[2]*Department of Physics, Visva Bharati University, Santiniketan 731235, West Bengal, India*

[3]*School of Electrical Sciences, Indian Institute of Technology, Bhubaneswar 751013, India*

(Received 18 April 2012; published 29 August 2012)

A density functional theory study of substitutional carbon impurities in ZnO has been performed, using both the generalized gradient approximation (GGA) and a hybrid functional (HSE06) as exchange-correlation functional. It is found that the nonspinpolarized C_{Zn} impurity is under almost all conditions thermodynamically more stable than the C_O impurity which has a magnetic moment of $2\mu_B$, with the exception of very O-poor and C-rich conditions. This explains the experimental difficulties in sample preparation in order to realize d^0 ferromagnetism in C-doped ZnO. From GGA calculations with large 96-atom supercells, we conclude that two C_O-C_O impurities in ZnO interact ferromagnetically, but the interaction is found to be short-ranged and anisotropic, much stronger within the hexagonal *ab* plane of wurtzite ZnO than along the *c* axis. This layered ferromagnetism is attributed to the anisotropy of the dispersion of carbon impurity bands near the Fermi level for C_O impurities in ZnO. From the calculated results, we derive that a C_O concentration between 2% and 6% should be optimal to achieve d^0-ferromagnetism in C-doped ZnO.

DOI: 10.1103/PhysRevB.86.054441 PACS number(s): 75.50.Pp, 71.15.Mb, 61.72.S−

I. INTRODUCTION

Ferromagnetism is a quantum phenomenon which arises from the long range ordering of interacting magnetic moments in a solid. The richness of magnetic properties in solids is due to hybridization of *d* and *f* orbitals which is decisive for magnetic moment formation and the way individual moments interact with each other in the solid. This is one of the reasons why magnetic semiconductors or diluted magnetic semiconductors (DMS) are traditionally conceived as semiconducting materials with transition metal ions as dopant. Numerous studies of DMS, both experimental and theoretical (see, e.g., Refs. 1–5) have come up with varying conclusions. In ZnO, substituting the cation by an isovalent transition metal, e.g., cobalt, introduces magnetic moments, but in itself does not lead to ferromagnetic coupling between these moments.[5] Hence, complex strategies, for instance co-doping, and elaborate growth techniques seem to be necessary to fabricate a DMS based on ZnO as host material.

Recently there are reports on magnetism in semiconducting materials without any *d* or *f* elements.[6–9] This is commonly known as d^0 magnetism and discussed for different classes of materials, starting from pure carbon based materials like graphite, graphene, and nonmetallic nanoparticles.[10,11] The common feature in this class of materials is that magnetism involves the $2p$ orbitals. The origin of magnetic moment is attributed to incomplete cancellation of majority and minority spin electronic contribution due to the Hund's type exchange. Magnetic moments have been reported for almost all ionic semiconductors in the presence of intrinsic defects, such as cation vacancies, or in the presence of impurities related to anion substitution. In the following we discuss reports of magnetism in semiconductors with impurities at the anion site.

The formation of a localized magnetic moment, which is a prerequisite for d^0 magnetism, depends on the relative strength of electronegativity between the dopant element and the anion of the host semiconductor. If the bond between the dopant and the cation is weaker than the native bond of the semiconductor, this leads to localized atomic-like $2p$ orbitals of the dopant and a stable spin-polarized state. On the other hand, if the strength of the bond is stronger than the native bond of the semiconductor, this will cause delocalization of the dopant $2p$ orbitals due to strong hybridization with the cations. Consequently, there is reduced or vanishing spin polarization in the system.[12] Hence, substituting the anion site by an element with smaller electronegativity can introduce spin-polarized states in the gap which can then mediate the magnetic interaction through the double-exchange mechanism as discussed by Mavropoulos *et al.*[13]

By means of DFT calculations, Peng *et al.*[14] have shown that many elements in the second row of the periodic table ($X = B, N, C$) when substituted at the anion site can develop a spin-polarized solution in AlN (X_N) and ZnO (X_O). However, the nature of the magnetic correlation in the case of B_O and N_O is still under debate.[14–17] Specifically for ZnO, Adeagbo *et al.* found that both N_O and N_{Zn} develop spin polarization with almost 1 μ_B/N in ZnO.[18] Lyons *et al.* have studied N_O in ZnO by hybrid-functional calculations and observed that N_O defects create a deep impurity state.[19] These states, if partially filled, can be spin polarized. Also for C_O, DFT calculations predicted a magnetic moment for the neutral or singly charged impurity.[20] There are experimental reports of room temperature ferromagnetism in carbon-doped ZnO films grown by pulsed-laser deposition.[21,22] Measurements of the anomalous Hall effect have shown that the ferromagnetism is mediated by the charge carriers in ZnO. Remarkably, results have been reported both for samples showing *n*-type conductivity[21] and *p*-type conductivity.[23] Moreover, Yi *et al.* reported on room-temperature ferromagnetism in carbon doped ZnO films when co-doped with nitrogen.[24]

In this work, we select ZnO as a host material for the study of d^0 magnetism. Impurities and defects in ZnO have been an active topic of research.[25,26] Here we focus on the magnetic properties of ZnO with carbon as a substitutional impurity (on the zinc site denoted by C_{Zn}, and on the oxygen

site denoted by C_O) studied with the help of density functional theory (DFT) calculations. The paper is arranged as follows: In the next section we present technical details of our DFT calculations. Section III discusses the stability of carbon impurities in ZnO by calculating their formation energies. The distance-dependent exchange constants of C_O in ZnO are obtained from the total energy differences of ferromagnetic and antiferromagnetic states. Finally, we conclude on the possible connection between C impurities and the ferromagnetism in ZnO found in experiments.

II. COMPUTATIONAL DETAILS

Electronic structure calculations are performed using the plane-wave pseudopotential DFT method as implemented in the Vienna *ab initio* simulation package (VASP).[27,28] For studying a substitutional impurity in ZnO, the system is modeled as a supercell consisting of periodic repetitions of the primitive wurtzite cell. Since we use different sizes of supercells, we stick to a particular nomenclature in our discussions. We refer to the size of the supercell with periodic extension $n_x \times n_y \times n_z$ as "S$n_x n_y n_z$." The electronic structure of homogeneously distributed impurities has been studied with the relatively small supercell S222, see Fig. 1(c), while to study impurity pairs in ZnO we employ two kinds of large supercells, namely S622 and S226 [Figs. 1(d) and 1(e)], respectively. This is necessary as the wurtzite crystal structure is noncentrosymmetric and the bond lengths are different along the hexagonal plane and along the c direction. Essentially, S622 intends to scan the interactions along the hexagonal plane of the lattice and the S226 scans the interaction along the c axis of the lattice.

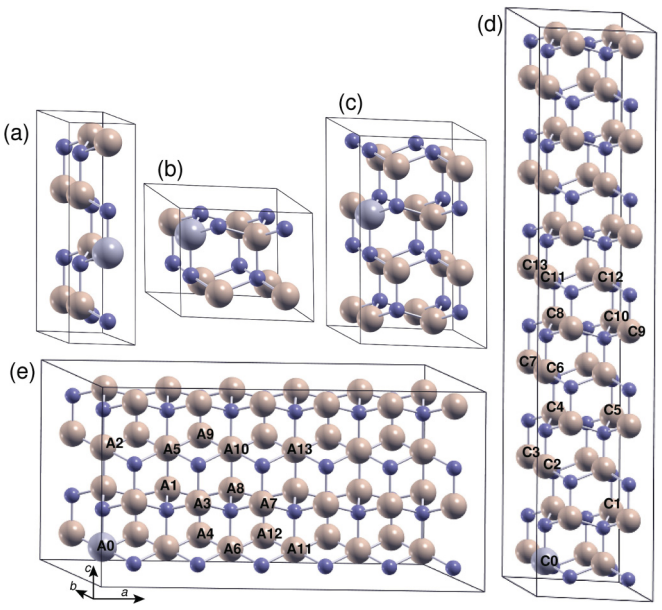

FIG. 1. (Color online) Supercells and impurity configurations used in the present study. The small (indigo) spheres represent Zn, and among the large spheres, the darker ones represent carbon on the O sites while light spheres represent oxygen atoms in the ZnO lattice. The supercells S122 (a), S221 (b), and S222 (c) contain a single impurity and are used to model impurity concentrations of 12.5% for S122 and S221 and 6.25% for S222. The C_O-C_O interaction is studied with two C_O in S226 (d) and S622 (e): One of them fixed at the position C0 and A0 in S226 and S622, respectively, and another placed on one of the C1–C13/A1–A13 sites, which corresponds to a concentration of 4.17%.

The calculations have been performed using a plane-wave energy cutoff of 400 eV. We have used the generalized gradient approximation (GGA) with the PW91 parameterization[29] for the exchange-correlation potential, and the ion-electron interactions are treated with the projector-augmented wave (PAW) method.[30] The lattice constants of the primitive lattice of ZnO are taken to be $a = 3.29$ Å, $c/a = 1.606$, and the relative shift of Zn and O planes, $u = 0.380$, which were found to be the minimum energy lattice parameters in the GGA calculations.[31] The doped supercell configuration is relaxed to avoid any strain until the structural energy is converged to 10^{-6} eV. At this level of tolerance, the forces in the system are found to be below 3×10^{-4} eV Å^{-1}. The relaxation is performed with a Γ-centered Monkhorst-Pack k-points grid of $3 \times 5 \times 5$ and $5 \times 5 \times 3$ for supercells S622 and S226, respectively.

Part of these results have been cross-checked with the full-potential local orbital (FPLO) minimum-basis code, which uses localized basis sets.[32] DFT within GGA gives reliable structural parameters for ZnO but has limitation in predicting the right optical band gap, which is with a value of 0.69 eV grossly underestimated in comparison to the experimental value of 3.4 eV.[31] In addition, the localization of Zn d bands is not properly described by GGA because the hybridization of Zn d and O p bands is overestimated. Thus, the Zn d bands are located almost 3 eV too close to the Fermi level as compared to experimental observation.[33] This is frequently corrected pragmatically within the GGA + U approach, where an empirical Hubbard-U term is added to the Hamiltonian for Zn d orbitals ($U_d = 7.5$ eV). This shifts the Zn d orbitals to the experimental position below the band gap and also improves the band gap.[31] Another way to overcome the problem is through the introduction of hybrid functionals where the electronic exchange potential is mixed with some percentage of Hartree-Fock exchange, while the electronic correlation potential is entirely taken from the GGA. This leads to a better description of the gap and the Zn-d states move to better positions too. We have employed the screened hybrid functionals to ascertain the electronic structure of a single impurity. The hybrid functionals are of the type suggested by Heyd, Scuseria, and Ernzerhof,[34] with the exact (Hartree-Fock) exchange and the GGA exchange in the ratio 1:3.[35] We have used the HSE06 functional for our studies.[36]

III. RESULTS AND DISCUSSION

The stability of an impurity configuration can be judged from its formation energy. Since substitution changes the number of atomic species, the formation energy must be calculated with reference to thermodynamic reservoirs characterized by their chemical potentials. In practice, the values of these chemical potentials reflect the experimental conditions during sample preparation. The formation energy E_f is thus defined as

$$E_f = E_{\mathrm{Tot}} - E_{\mathrm{ZnO}} - \sum_i n_i \mu_i, \qquad (1)$$

where E_{Tot} is the total energy of the supercell with impurity, E_{ZnO} is the energy of the pure ZnO host with the equivalent number of stoichiometric ZnO units, μ_i is the chemical potential of a species, and n_i is the change of number of the corresponding species in the supercell. In thermodynamic equilibrium with bulk ZnO, the condition

$$\mu_{\mathrm{ZnO}} = \mu_{\mathrm{O}} + \mu_{\mathrm{Zn}} \tag{2}$$

must always be satisfied. This leaves us with just one unknown, which we choose to be μ_{O}. However, an interval for the values of μ_{O} corresponding to physically meaningful growth conditions can be provided: The upper bound of the chemical potential, corresponding to O-rich growth conditions, is taken from the oxygen molecule $\mu_{\mathrm{O}} = \frac{1}{2}E_{\mathrm{O}_2}$. Oxygen-poor conditions (or, equivalently, Zn-rich conditions) correspond to the equilibrium with metallic bulk Zn, $\mu_{\mathrm{Zn}} = E_{\mathrm{Zn}}^{\mathrm{bulk}}$, and hence, from Eq. (2), $\mu_{\mathrm{O}} = \mu_{\mathrm{ZnO}} - E_{\mathrm{Zn}}^{\mathrm{bulk}}$.

A. C_{Zn} and C_O impurities

The formation energies of carbon at the Zn-site (C_{Zn}) and at the O-site (C_{O}) obtained from calculations with a $3 \times 3 \times 3$ supercell of ZnO are summarized in Table I for two different environments. The limiting chemical potentials of the C-rich and for C-poor cases are taken as $\mu_{\mathrm{C}} = E_{\mathrm{C}}^{\mathrm{atomic}}$ and $\mu_{\mathrm{C}} = E_{\mathrm{CO}} - \frac{1}{2}E_{\mathrm{O}_2}$, respectively, as described in Ref. 20. We note that the deviation of the values as compared to Ref. 20 is due to the different exchange-correlation functionals used in both calculations. The values obtained by Tan *et al.*[37] should not be directly compared to ours because they have used the total energies of single atoms as reference chemical potentials. In Fig. 2, the formation energies which we obtain for C_{O} and C_{Zn} impurities are plotted as a function of oxygen chemical potential. Our formation energies suggest that C_{O} and C_{Zn} impurities are energetically favorable only under carbon-rich conditions (negative values in the formation energy). Also, the formation energy of C_{Zn} is smaller than the formation energy of C_{O} in all chemical environments.

We find that the formation of C_{O} is energetically favorable only in a narrow range of μ_{O} shown as the thick (blue) vertical line. This tiny region corresponds to an equilibrium with metallic zinc, i.e., extremely O-poor conditions. Hence stabilizing the C_{O} defect in ZnO is difficult under common experimental growth conditions of high oxygen pressure where μ_{O} approaches the value corresponding to molecular oxygen.

A single C_{O} in a ZnO supercell leads to a spin-polarized solution with an integral magnetic moment of $2\mu_B$/C as discussed in the literature previously.[12,21,38] The spin polarized solution is lower in energy than the nonspin polarized one by a difference of 0.215 eV. The corresponding density of states (DOS) of C_{O} as a single impurity in supercell S222 is shown in Figs. 3(d)–3(f), employing the GGA, GGA + U_d, and HSE06

TABLE I. Formation energy of C_{O} and C_{Zn} calculated from Eq. (1). The data show that the C_{Zn} impurity is thermodynamically more stable than the C_{O} impurity.

		Carbon rich	Carbon poor
O poor,	C_{O}	−4.558	4.070
	C_{Zn}	−4.576	4.052 (4.0, Ref. 37)
O rich,	C_{O}	−1.569 (0.4, Ref. 20)	7.059 (9.4, Ref. 20)
	C_{Zn}	−7.564 (−6.2, Ref. 20)	1.064 (2.8, Ref. 20; 2.2, Ref. 37)

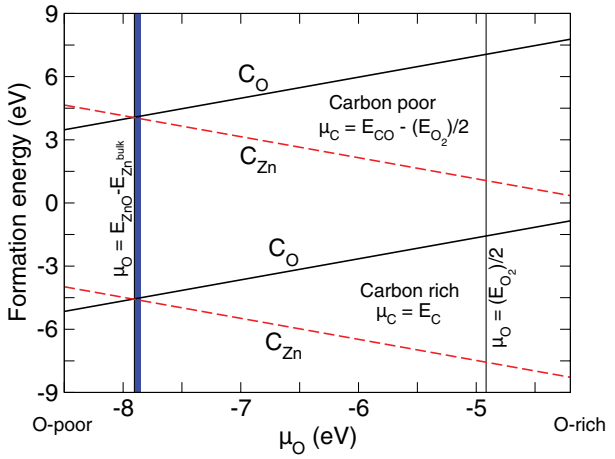

FIG. 2. (Color online) The formation energy of C_{O} and C_{Zn} defects as a function of μ_{O}. The thick vertical line (blue colored line) shows the narrow range where the C_{O} impurity can compete with C_{Zn}.

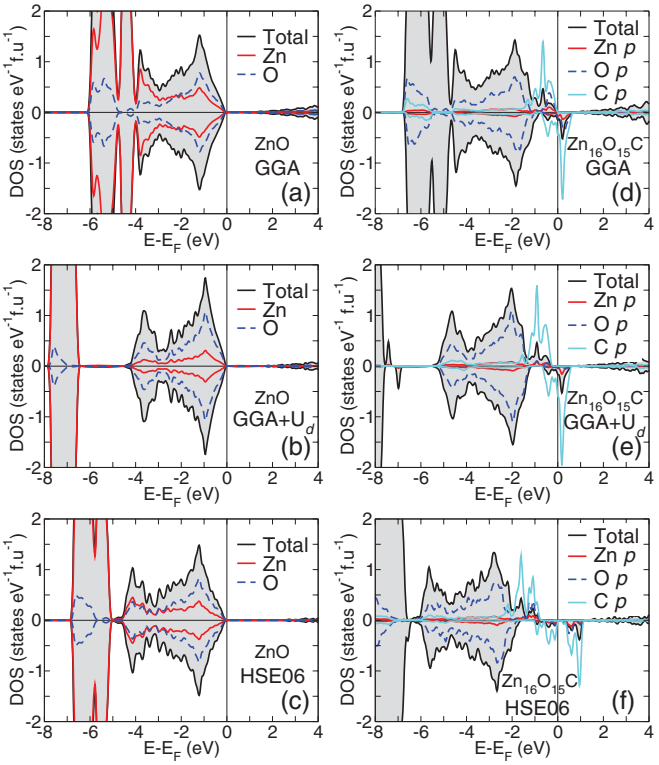

FIG. 3. (Color online) Density of states (DOS) of pure ZnO [(a)–(c)] and C_{O} impurity in ZnO [(d)–(f)]. The DOS in different rows are obtained from GGA, GGA + U_d on Zn, and from HSE06 functional. The spin-up DOS and the spin-down DOS are plotted as positive and negative y axis. The DOS of C_{O} impurity in ZnO in S222 geometry consists of the atomic contribution of nearest neighbor Zn, O to C in units of states/atom, while the total DOS is scaled to the number of formula units of ZnO.

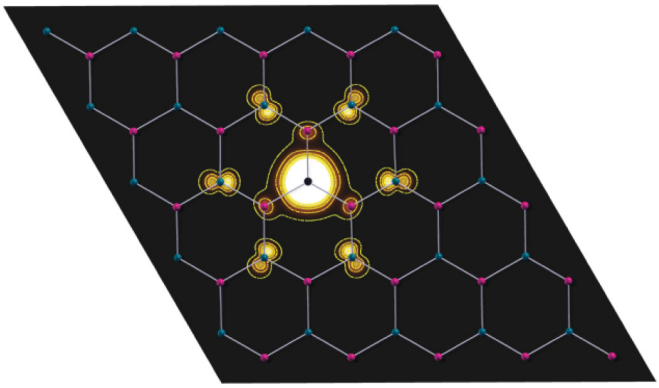

FIG. 4. (Color online) Effective spin density ($\Delta\rho = \rho_\uparrow - \rho_\downarrow$) plotted along the plane perpendicular to c axis and passing through C_O. The light (magenta), dark (turquoise), and black colored balls are used to represent Zn, O, and C atoms (Ref. 42). The isolines (and also the color gradient) are plotted from 0.003 eÅ^{-3} to 0.028 eÅ^{-3} at intervals of 0.005 eÅ^{-3}. One can clearly observe that the spin-polarization arising from C_O extends to a relatively large spatial region.

functionals. For comparison, the DOS of pure ZnO obtained from each method is shown in Figs. 3(a)–3(c). In GGA + U_d, the value $U_d = 7.5$ eV is applied to the (fully occupied) Zn d orbitals. We find a magnetic solution for C_O in all the methods. Note that both in GGA + U_d and in HSE06, the impurity band in the minority spin is clearly separated from the valence band. The real-space plot of the effective spin density (from GGA) obtained by subtracting the charge densities of majority and minority spins ($\Delta\rho = \rho_\uparrow - \rho_\downarrow$) is shown in Fig. 4. One finds that the effective spin density is centered on the C atom and extends to the nearest neighbor Zn atoms and the next-nearest neighbor O atoms with a total magnetic moment of $2\mu_B$/C. We note that the HSE06 functional gives a large exchange splitting of the impurity states and larger band gap for ZnO than GGA, and the impurity states introduced by C_O which mainly consist of carbon states are deep in the gap when measured from the valence band maximum (VBM). Therefore, it is not possible to use C_O as an acceptor that could introduce hole states for thermally activated p-type conductivity in ZnO. On the other hand, the more stable C_{Zn} impurity acts as a donor and does not lead to any spin polarization, in agreement with Ref. 39.

Finally, we discuss possible compensation effects that could alter the magnetic properties of C_O. Using DFT studies, Li *et al.* have shown that the presence of oxygen vacancy (V_O) quenches the spin polarization from C_O in ZnO.[40] Comparing the formation energy of neutral defects,[41] we conclude that both V_O and V_{Zn} have positive formation energy, with the formation energy of V_O being lower than the formation energy of V_{Zn} in O-poor conditions (favorable conditions for C_O as seen above). Hence, the role of defects like V_{Zn} and V_O can be safely ruled out in contributing to magnetism in the material. However, the magnetic moment of C_O can be quenched by H impurities in ZnO that act as donor. We have tested co-doping of H and C in S622 and find that the electron from H compensates one Bohr magneton of magnetic moment. Upon adding two H in the supercell, the magnetic moment is completely quenched to zero. This observation is independent of the distance of the hydrogen from the carbon site in the supercell. In experiments the hydrogen concentration during ZnO synthesis is difficult to control. It has been found that the energy barrier for the escape of H through the ZnO surface can be as large as 0.58 eV.[43] Thus even if one succeeds with C_O doping, one may still fail to obtain magnetic moments due to the ubiquitous presence of hydrogen. Similar conclusions have also been derived from formation energy studies.[44]

B. Fixed spin moment calculations using supercell approach

Although the thermodynamic stability considerations of the previous section point to the difficulty in incorporating larger amounts of carbon on the oxygen site in ZnO, we continue to discuss the consequences of C_O impurities for the magnetic properties, assuming that an appreciable concentration can be built up by nonequilibrium preparation techniques. In order to investigate impurity interactions at various concentrations, we perform DFT calculations with both VASP and FPLO using a single C_O impurity in the different supercells shown in Figs. 1(a)–1(c). These cells correspond to carbon concentrations of 12.5% (for both S122 and S221) and 6.25% (S222). Upon decreasing the C concentration from 12.5% to 6.25%, the interaction between impurities becomes weaker and the impurity band becomes narrower. Even though the supercells S221 and S122 have the same doping concentration of 12.5%, they do not lead to equivalent electronic structure because the distance of separation of the C_O impurity with its periodic image is different since the lattice parameter c is longer than the lattice parameter a in a wurtzite crystal structure. From Table II, we note that the magnetic moment of S122 is a fractional value in units of μ_B, an indication of strong hybridization between the C $2p$ orbitals and the valence band, leading to metallic behavior as shown in the DOS of Fig. 5(a). However, the magnetic moment of S221 and S222 is integer (2 μ_B), i.e., the system is a magnetic half-metal [see Figs. 5(b) and 5(c)]. We carried out fixed-spin-moment (FSM) calculations to test the stability and characteristics of the spin-polarized solutions itself. The plot in Fig. 6 shows the magnetic polarization energy of the supercells shown in Figs. 1(a)–1(c). Here the

TABLE II. Nearest neighbor (nn) and next-nearest neighbor (nnn) distance of the periodic image of the C impurity in Å, magnetic moments as obtained from VASP (FPLO), and formation energy (E_f) for O-poor and C-rich conditions. The total magnetic moment (M_{Total}) is shown per supercell, while the magnetic moments of Zn (M_{Zn}) and O (M_O) are shown per atom, averaged over the nearest neighbor Zn and O, respectively.

Supercell	r_{nn} (Å)	r_{nnn} (Å)	M_{Total} (μ_B)	M_C (μ_B)	M_{Zn} (μ_B)	M_O (μ_B)	E_f (eV)
S122	3.290	6.580	0.953 (1.194)	0.300 (0.743)	0.049 (0.072)	0.0465 (0.061)	−4.009
S221	5.284	6.580	2.000 (2.000)	0.591 (1.235)	0.118 (0.076)	0.0085 (0.081)	−3.758
S222	6.580	10.57	2.000 (2.000)	0.584 (1.235)	0.118 (0.045)	0.0068 (0.058)	−3.910

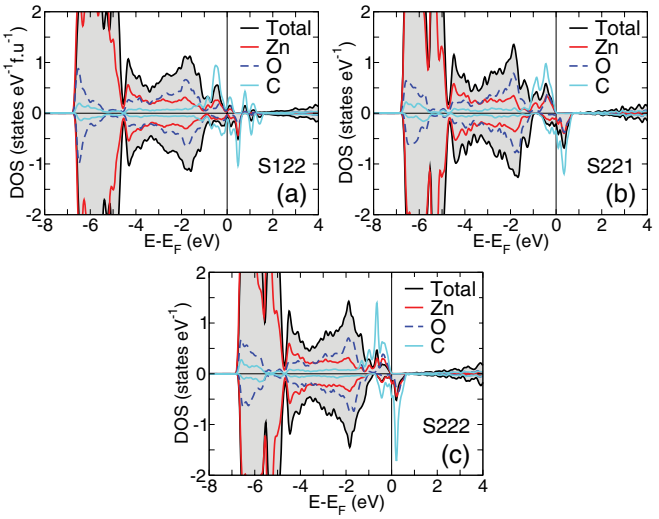

FIG. 5. (Color online) DOS of C_O in supercells S122 (a), S221 (b), and S222 (c), respectively. The DOS consists of the atomic contribution of nearest neighbor Zn and O to C (in units of states/atom), while the total DOS is scaled to the number of formula units of ZnO.

magnetic polarization energy is defined as the energy of the system at a given fixed magnetic moment (m) relative to the energy of nonmagnetic solutions ($m = 0$). When a spin-polarized solution is favored, the magnetic polarization energy takes negative values. For metallic systems (supercell S122), the minimum magnetic polarization energies are found at noninteger values of m as shown in Table II, and the magnetic polarization energies show a smooth parabolic change around the minima. For supercells S221 and S222 the minimum magnetic polarization energy is obtained at an integer value $m = 2\ \mu_B$, and the energy has a cusp at the minima which is due to the localized impurity band in the gap. Thus, from the

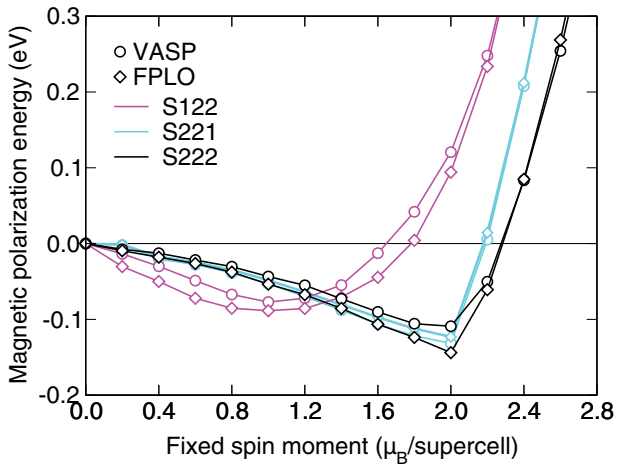

FIG. 6. (Color online) Magnetic polarization energy ($E_{sp} - E_{nsp}$) (sp = spin polarized and nsp = nonspin polarized) as a function of the magnetic moment for different supercells from fixed-spin-moment (FSM) calculations. The minima in the magnetic polarization energy indicate the most stable magnetic moment in the supercell. The magnetic polarization energies obtained from VASP and that of FPLO are in close agreement with each other.

FSM calculations we verify the stability and characteristics of spin-polarized solutions in the supercells, and one can estimate an upper bound of C concentration for the material to be a semiconductor rather than a metal. A higher C concentration leads to a metallic solution, i.e., the impurity band hybridizes with the valence band of ZnO. According to the GGA results, the distance between C impurities should be larger than twice the lattice constant, meaning that the C concentration should be lower than 6%, to avoid such a metallic state. The precise estimate of this concentration might depend on the exchange-correlation functional used in the calculations. As we discussed above, hybrid functionals predict the impurity bands to lie further up in the gap. Consequently, ZnO may tolerate an even larger C concentration before becoming metallic than the values we have estimated from the GGA.

C. Distance dependent exchange constant in C-doped ZnO

Next, we study the magnetic interaction between the carbon impurities as a function of their separation. We employ the relatively large supercells S622 and S226 [Figs. 1(d) and 1(e)] with two C_O in the supercell to include the long-range interactions. The concentration of carbon in these supercells is 4.17% which is within the range of experimental impurity concentrations.[21] As long as the carbon impurities are well separated (maximum separation of 16 Å in the c direction and 11 Å in the ab direction for S226 and S622, respectively), each impurity retains its magnetic moment of $2\mu_B$ independent of the distance.

The nature and strength of the magnetic interaction can be ascertained by comparing the total energies of the ferromagnetic and the antiferromagnetic alignment of carbon spins, since the energy differences obtained from the different magnetic configurations is proportional to the exchange constant. We obtain the effective exchange constant for a pair of C_O from the total energy difference $E_{AFM} - E_{FM}$, where E_{AFM} and E_{FM} are the total energies for the antiferromagnetic and the ferromagnetic alignment of the impurity spins in the supercell. In principle, the energy difference contains all exchange interactions of the infinite lattice together with the periodic arrangement of the impurities. If the separation of the carbon atoms in the primary supercell is equal to the separation of a carbon atom in the primary supercell and the periodic images of the other carbon atom, then in these cases the magnetic interactions are overestimated by the number of such impurity pairs (note that the contributions from the periodic images of the same atom cancel out in the energy difference). Since the magnetic interaction is short ranged in the DMS systems, it is reasonable to retain only nearest neighbor interactions between the impurities. The number of nearest neighbor impurities is represented by n_p. Thus, one must divide the total energy difference by a factor n_p. This leads to

$$J_{0i} = \frac{E_{AFM} - E_{FM}}{n_p}, \tag{3}$$

where the 0 is a fixed carbon site and i is the different configurations of the second carbon atom used in separate calculations using the same supercell. In this form, $J_{0i} > 0$ implies stability of ferromagnetic interaction.

In the supercells S226 and S622, choosing one C atom as the origin [represented as 0: C0 and A0 in Figs. 1(d) and 1(e)]

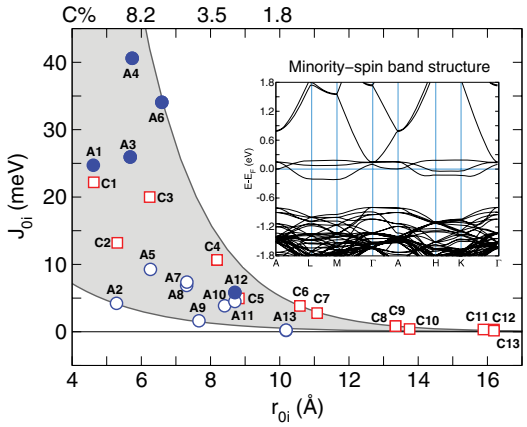

FIG. 7. (Color online) Exchange constant extracted from the total energy using Eq. (3) plotted against the relaxed C_O-C_O distance. C1–C13 and A1–A13 represent the different positions of C_O in supercell S226 and S622 (represented as i) as in Figs. 1(d) and 1(e), with the other C_O positioned at C0 and A0 (represented as 0), respectively. The range of interaction values is bounded by two exponential curves. The J_{0i} for the C_O-C_O oriented along the ab-hexagonal plane, which are shown as filled symbols, are larger than those along the c axis. From the minority-spin band structure of a C_O impurity in ZnO (in GGA) shown in the inset one finds that the C_O band crosses the Fermi energy in the hexagonal plane (A–L, Γ–M, A–H and Γ–K directions) imparting metallic character, and thus the magnetic interactions along the hexagonal plane are stronger.

we estimated the exchange constants for different position vectors (r_{0i}) of the other C atom [represented as i: C1-C13 and A1-A13 in Figs. 1(d) and 1(e)]. The exchange constants $J_{0i}(r_{0i})$ obtained by this procedure are plotted in Fig. 7. As a guide to the eye, we include a shaded area bounded by two exponentially decaying functions within which all the interactions are contained. We note that the J_{0i} are positive in the whole range, i.e., the spin interaction between C_O is ferromagnetic in the host material. Averagely, the J_{0i} decrease with increasing separation r_{0i} between the impurities while there is a large spread in the data for small distances. We categorize the geometric configuration of the impurities using the crystallographic direction and select those configurations that have the major component of their distance vectors in the hexagonal plane (ab direction). The selected configurations (A1, A3, A4, A6, and A12) are shown as filled symbols in Fig. 7. We observe a strongly anisotropic behavior of J_{0i}: The filled symbols are located in the upper part of the shaded area, whereas the open symbols are in the lower part. Test calculations performed for some configurations with the GGA + U_d method have confirmed the ferromagnetic nature of the interactions and indicate that the results are independent of the exact energetic position of the minority-spin C $2p$ states within the host band gap.

Since the carbon impurity levels lie deep inside the band gap [see the DOS in Fig. 3(d)], the magnetic interactions cannot be mediated by carriers in the valence or conduction bands of the host material (as typical for small-gap DMS materials). Instead, ferromagnetism arises from partly filled impurity bands, as in Zener's double-exchange model.[13,45,46] According to this model, ferromagnetic ordering becomes stabilized because it allows for a lowering of the kinetic energy of the electrons in the impurity band: Due to the overlap of impurity orbitals of the same spin, the dispersion of the impurity bands is increased, and the kinetic energy of electrons occupying the lower part of these bands is decreased. Obviously, this energy gain is largest for interactions along those crystallographic directions where the impurity band crosses the Fermi level.

The anisotropic nature of the magnetic interaction can therefore be explained from the band structure of C_O in ZnO. In the inset of Fig. 7, the band structure of the minority spin states of C_O in S333 is shown. Since the spin-majority impurity bands are completely filled and thus cannot give rise to any energy gain, only the minority-spin bands can be responsible for the magnetic interactions. We find that the carbon bands are crossing the Fermi level mostly along the hexagonal ab plane, i.e., along the A–L, Γ–M, A–H, and Γ–K directions, while along the c axis (M–L, Γ–A, and K–H) the Fermi energy lies in the gap between the occupied and the unoccupied bands. Therefore, the ferromagnetic interaction is mediated more effectively within the hexagonal ab plane, giving rise to anisotropic ferromagnetism.

We note that the ferromagnetic interaction is rather short ranged (below 10 Å). Ferromagnetism at finite temperatures can thus only be expected at a carbon concentration larger than 2% (refer to the scale of the C concentration in the upper axis of Fig. 7). Together with the estimate given in Sec. III B, which gives the upper bound for C concentration to avoid metallic state, we conclude that a C_O concentration between 2% and 6% should be optimal to obtain ferromagnetism due to homogeneously distributed impurities. Moreover, we note that C impurities have a tendency to cluster which poses an upper limit to the useful concentration. As pointed out in previous work,[47] the C impurities tend to form energetically more stable C_2 molecules. In this case, the $pp\pi^*$ orbital of the C_2 molecule resonates with the conduction band of ZnO which may lead to ferromagnetism mediated by the host material in n-type ZnO. Thus, this mechanism differs from the ferromagnetic interaction between C_O impurities described in the present work which originates from conductivity due to impurity bands, and is hence independent of host carriers.

IV. CONCLUSIONS

We have studied the two possible substitutional carbon impurities in ZnO (C_O and C_{Zn}) and find that C_{Zn} is energetically more favorable than C_O. However, C_O can be stabilized under specific (O-poor and C-rich) growth conditions. This type of environment is uncommon in usual ZnO growth, but could be generated by oxidizing metallic zinc in the presence of an atomic carbon source. Given that a material with a C_O concentration of 2–6% can be realized, this would be an interesting prototypical system for d^0 magnetism: Our DFT calculations indicate that C_O in this range of concentrations is associated with a localized magnetic moment of 2 μ_B/C. Partially filled impurity bands in the minority spin channel mediate ferromagnetic interaction between the C_O impurities. These interactions are short-ranged and anisotropic, being stronger within the ab-plane of the wurtzite ZnO crystal than along the c axis. Based on our calculations, we predict that such layered ferromagnetism could be used as an experimental

hallmark to distinguish carbon-induced magnetism from possible other forms of defect-induced ferromagnetism in ZnO.

ACKNOWLEDGMENTS

We thank Alfred Hucht, Andreas Ney, and Heike Herper at University of Duisburg-Essen for fruitful discussions. We acknowledge the computational resources from Center for Computational Sciences and Simulation (CCSS), University of Duisburg-Essen. The work was funded by Deutsche Forschungsgemeinschaft through the Research Training Group GRK-1240 "Photovoltaics and Optoelectronics from Nanoparticles."

*sanjeev.nayak@uni-due.de

†Emeritus Professor at National Institute of Science and Technology, Palur Hills, Berhampur 761008, India;deceased.

[1] C. Liu, Fi. Yun, and H. Morkoç, J. Mater. Sci.: Mater. Electron. **16**, 555 (2005).

[2] S. J. Pearton, C. R. Abernathy, M. E. Overberg, G. T. Thaler, D. P. Norton, N. Theoderopoulou, A. F. Hebard, Y. D. Park, F. Ren, J. Kim, and L. A. Boatner, J. Appl. Phys. **93**, 1 (2003).

[3] K. Sato, L. Bergqvist, J. Kudrnovský, P. H. Dederichs, O. Eriksson, I. Turek, B. Sanyal, G. Bouzerar, H. Katayama-Yoshida, V. A. Dinh, T. Fukushima, H. Kizaki, and R. Zeller, Rev. Mod. Phys. **82**, 1633 (2010).

[4] T. Dietl, Nat. Mater. **9**, 965 (2010).

[5] A. Ney, Materials **3**, 3565 (2010).

[6] K. Kenmochi, M. Seike, K. Sato, A. Yanase, and H. Katayama-Yoshida, Jpn. J. Appl. Phys. **43**, L934 (2004).

[7] M. Venkatesan, C. B. Fitzgerald, and J. M. D. Coey, Nature (London) **430**, 630 (2004).

[8] A. L. Ivanovskii, Phys. Usp. **50**, 1031 (2007).

[9] O. Volnianska and P. Boguslawshi, J. Phys.: Condens. Matter **22**, 073202 (2010).

[10] P. Esquinazi, D. Spemann, R. Höhne, A. Setzer, K-H. Han, and T. Butz, Phys. Rev. Lett. **91**, 227201 (2003).

[11] *Carbon-based magnetism: An overview of metal free carbon-based compounds and materials*, edited by T. Makarova and F. Palacio (Elsevier, Amsterdam, 2006).

[12] K. Yang, R. Wu, L. Shen, Y. P. Feng, Y. Dai, and B. Huang, Phys. Rev. B **81**, 125211 (2010).

[13] P. Mavropoulos, M. Ležaić, and S. Blügel, Phys. Rev. B **80**, 184403 (2009).

[14] X. Peng and R. Ahuja, Appl. Phys. Lett. **94**, 102504 (2009).

[15] I. S. Elfimov, A. Rusydi, S. I. Csiszar, Z. Hu, H. H. Hsieh, H.-J. Lin, C. T. Chen, R. Liang, and G. A. Sawatzky, Phys. Rev. Lett. **98**, 137202 (2007).

[16] L. Shen, R. Q. Wu, H. Pan, G. W. Peng, M. Yang, Z. D. Sha, and Y. P. Feng, Phys. Rev. B **78**, 073306 (2008).

[17] H. Peng, H. J. Xiang, S.-H. Wei, S.-S. Li, J.-B. Xia, and J. Li, Phys. Rev. Lett. **102**, 017201 (2009).

[18] W. A. Adeagbo, G. Fischer, A. Ernst, and W. Hergert, J. Phys.: Condens. Matter **22**, 436002 (2010).

[19] J. L. Lyons, A. Janotti, and C. G. Van de Walle, Appl. Phys. Lett. **95**, 252105 (2009).

[20] S. Sakong and P. Kratzer, Semicond. Sci. Technol. **26**, 014038 (2011).

[21] H. Pan, J. B. Yi, L. Shen, R. Q. Wu, J. H. Yang, J. Y. Lin, Y. P. Feng, J. Ding, L. H. Van, and J. H. Yin, Phys. Rev. Lett. **99**, 127201 (2007).

[22] S. Zhou, Q. Xu, K. Potzger, G. Talut, R. Grötzschel, J. Fassbender, M. Vinnichenko, J. Grenzer, M. Helm, H. Hochmuth, M. Lorenz, M. Grundmann, and H. Schmidt, Appl. Phys. Lett. **93**, 232507 (2008).

[23] T. S. Herng, S. P. Lau, L. Wang, B. C. Zhao, S. F. Yu, M. Tanemura, A. Akaike, and K. S. Teng, Appl. Phys. Lett. **95**, 012505 (2009).

[24] J. B. Yi, L. Shen, H. Pan, L. H. Van, S. Thongmee, J. F. Hu, Y. W. Ma, J. Ding, and Y. P. Feng, J. Appl. Phys. **105**, 07C513 (2009).

[25] M. D. McCluskey and S. J. Jokela, J. Appl. Phys. **106**, 071101 (2009).

[26] S. B. Ogale, Adv. Mater. **22**, 3125 (2010).

[27] G. Kresse and J. Furthmüller, Comput. Mater. Sci. **6**, 15 (1996).

[28] G. Kresse and J. Furthmüller, Phys. Rev. B **54**, 11169 (1996).

[29] J. P. Perdew, *Electronic Structure of Solids '91*, edited by P. Ziesche and H. Eschrig (Akademie, Berlin, 1991).

[30] G. Kresse and D. Joubert, Phys. Rev. B **59**, 1758 (1999).

[31] S. K. Nayak, M. Ogura, A. Hucht, H. Akai, and P. Entel, J. Phys.: Condens. Matter **21**, 064238 (2009).

[32] K. Koepernik and H. Eschrig, Phys. Rev. B **59**, 1743 (1999).

[33] R. A. Powell, W. E. Spicer, and J. C. McMenamin, Phys. Rev. Lett. **27**, 97 (1971).

[34] J. Heyd, G. E. Scuseria, and M. Ernzerhof, J. Chem. Phys. **118**, 8207 (2003).

[35] J. P. Perdew, M. Ernzerhof, and K. Burke, J. Chem. Phys. **105**, 9982 (1996).

[36] J. Paier, M. Marsman, K. Hummer, G. Kresse, I. C. Ferber, and J. G. Ángyán, J. Chem. Phys. **125**, 249901 (2006).

[37] S. T. Tan, X. W. Sun, Z. G. Yu, P. Wu, G. Q. Lo, and D. L. Kwong, Appl. Phys. Lett. **91**, 072101 (2007).

[38] X.-L. Lin, S.-S. Yan, M.-W. Thao, S.-J. Hu, X.-X. Yao, C. Han, Y.-X. Chen, G.-L. Liu, Y.-Y. Dai, and L.-M. Mei, J. Appl. Phys. **107**, 033903 (2010).

[39] S. Papan, S. Xiyu, H. Qinying, L. Yodong, and C. Wei, J. Semicond. **30**, 052001 (2009).

[40] W. Q. Li, J. X. Cao, J. W. Ding, and Xuedong Hu, J. Appl. Phys. **110**, 123908 (2011)

[41] A. Janotti and C. G. Van de Walle, Phys. Rev. B **76**, 165202 (2007).

[42] A. Kokalj, Comput. Mater. Sci. **28**, 155 (2003) (code available at http://www.xcrysden.org/).

[43] J. J. Lander, J. Phys. Chem. Solids **3**, 87 (1957).

[44] A. Pham, M. H. N. Assadi, Y. B. Zhang, A. B. Yu, and S. Li, J. Appl. Phys. **110**, 123917 (2011).

[45] H. Akai, Phys. Rev. Lett. **81**, 3002 (1998).

[46] P. H. Dederichs, K. Sato, and H. Katayama-Yoshida, Phase Transitions **78**, 851 (2005).

[47] H. Wu, A. Stroppa, S. Sakong, S. Picozzi, M. Scheffler, and P. Kratzer, Phys. Rev. Lett. **105**, 267203 (2010).